

TECHNIQUE TO MEASURE
MAGNETOSTRICTION OF THIN AND
ULTRA THIN FERROMAGNETIC FILMS

THESIS

Presented to the Graduate Council of
Texas State University-San Marcos
In Partial Fulfillment
of the Requirements

for the Degree

Master of SCIENCE

by

Jonathan André Garrett, B.S.

San Marcos, Texas
December 2008

COPYRIGHT

By

Jonathan André Garrett

2008

ACKNOWLEDGEMENTS

I would like to acknowledge my appreciation and gratitude of family members, Reginald Garrett, Dena Downey Garrett and Elmo Garrett for their support and assistance both physically and financially, for whom this document would not have been possible and to Dr. Winifred J. Hamilton, Assistant Professor and Director Environmental Section Chronic Disease Prevention, for the opportunity to reclaim my passion and love of knowing what it means to be a physicist.

Academically and professionally I owe a great debt of gratitude to Dr. Geerts, who took on the arduous task as my graduate advisor and to the individuals Dr. Spencer and Dr. Ventrice for serving as members on my committee and my gratitude to the faculty member of the Physics Department at Texas State University-San Marcos.

This manuscript was submitted on December 11, 2008

TABLE OF CONTENTS

	Page
ACKNOWLEDGEMENTS	iv
LIST OF TABLES	vii
LIST OF FIGURES.....	viii
CHAPTER	
1.0 INTRODUCTION.....	1
2.0 SAMPLE PREPARATION PROCESS	3
3.0 MAGNETIC PROPERTIES.....	6
3.1 SATURATION MAGNETIZATION	6
3.2 MAGNETIC ANISOTROPY.....	8
3.3 DEMAGNETIZING FIELDS	10
3.4 MAGNETOSTRICTION.....	10
3.5 DOMAIN WALLS	14
4.0 THE EFFECTS OF STRESS ON THE MAGNETIC HYSTERESIS.....	18
5.0 MAGMETOSTRICTION SETUP	23
5.1 PRINCIPLE OF THE SETUP.....	23
5.2 DEFLECTION COEFFICIENT	24
5.3 SAMPLE HOLDER.....	27
5.4 FOTONIC SENSOR.....	28
5.5 MAGNETIC FIELD VECTOR OF HELMHOLTZ COILS	30

5.6	AC POWER SUPPLY OF HELMHOLTZ COIL SETUP	32
5.7	JUNCTION BOX.....	33
5.8	DATA ACQUISITION BOARD (<i>DAQ</i>).....	34
5.9	OSCILLOSCOPE.....	36
5.10	CONTROL SOFTWARE: LAB-VIEW PROGRAM.....	36
6.0	MEASURED RESULTS.....	46
6.1	MAGNETO-ELASTIC EFFECT: GROUND WORK FOR MAGNETOSTRICTION MEASUREMENT.....	46
6.2	PRELIMINARY RESULTS FOR VARIOUS FILM THICKNESS....	48
7.0	Conclusion.....	51
Appendix 1 - OTHER PROPERTIES OF THE NICKEL IRON SYSTEM.....		53
Appendix 2 – SELF - RESONANCE COIL: HIGH FREQUENCY LIMITATIONS OF HELMHOLTZ COIL.....		55
BIBLIOGRAPHY.....		57

LIST OF FIGURES

Figure	Page
1: Phase diagram for NiFe system.....	4
2: Saturation induction as a function of the nickel concentration for two different temperatures NiFe[16]	7
3: Ordered Ni ₃ Fe Crystalline Structure (FCC).....	8
4: Crystal anisotropy constant as a function of nickel concentration for FCC NiFe.....	9
5: The magnetostriction in (a) disordered (paramagnetic regime); (b) the demagnetized ferromagnetic regime; (c) the magnetized ferromagnetic state (saturation magnetization). 12	12
6: Magnetostriction from single crystalline (left) and polycrystalline NiFe.....	13
7: Curie temperature as a function of Nickel concentration.....	16
8: Kerr effects grey to right magnetic moments and white to the left.....	17
9: Easy axis along the [100] plane for NiFe-31	19
10: Localized and Global Strain.....	22
11: (a) Rectangular sample unstrained state (b) Strain state of rectangular sample.....	26
12: Optical Sensor and Sample Holder Setup.....	28
13: The front face of the MT-2000 Fotonic Sensor	28
14: The Probe to-Target Displacement of the receiving and transmitting optical fibers in relation to the plane of the sample.....	29
15: Maximum Optical peak for distance of optical device to film sample.....	29
16: The Inner and Outer Helmholtz Coils, deconstructed.....	31
17: The front and back panel of the Carver MT1.0T Magnetic Amplifier.....	33
18: The electrical hardware between the Carver MT1.0T Magnetic amplifier and the system of Helmholtz coils	34

19: An illustration of the breadboard, which serves as an electrical contact between the National Instruments PCI-GPIB board and the external hardware	35
20: Analog to Digital conversion process for the PCI-GPIB Board.....	36
21: Source code for the program “Direct Magnetostriction”	38
22: The main Lab-View VI Program to measure the Magnetostriction and Deflection coefficient as a function of time dependent Magnetic Induction fields	39
23: The "Magnetostriction" LabView VI Program to measure the Magnetostriction and Deflection coefficient as a function of time dependent Magnetic Induction field.....	41
24: The Object Oriented VI Program “WAAR”	43
25: The Front panel of the Lab-View Program “WAAR”	44
26: The Magneto-elastic Effect of a 500nm thick 31% NiFe sample	46
27: The Magneto-elastic Effect for Thin and Thick Ferromagnetic Film.....	47
28: Hysteresis curve of the Deflection of various samples of 31% sample of NiFe.....	48
29: The Measured Deflection as a function of applied fields for various samples of 31-NiFe.	49
30: Anisotropic Field versus Film Thickness.....	5

LIST OF TABLES

Tables	Page
1: Sample preparation of 31-NiFe on Silicon Wafer	5
2: Electrical properties of components inside Junction Box	33

CHAPTER 1

INTRODUCTION

Since IBM introduced the first hard drive in 1954, ferromagnetic material has steadily become an important material to store large amounts of data. This first hard disk in their RAMAC 305 computer contained fifty 24" disks, was capable of storing 5 million characters, and weighted over a ton. Fifty-four years later in 2008, Acron introduced its new mini hard drive that has a storage capacity of 500 Gbyte and a weight of just over 4 ounces. So a decrease of form factor of 10^9 in a little bit over 50 years which accounts for a doubling in information density each 21 months. Part of this large improvement is due to the introduction of a new type of reading head and the introduction of thin film techniques to produce them.

For the period of 1955 to 1970, magnetic material where an integral part of solid state memory devices. Small ferrite rings were used to store large amounts of data for computer applications. The cost per bit of this so called magnetic core memory declined sharply over the economic lifetime of this technology from \$1.00 a bit to \$0.01 at the end of the sixties. In the beginning of the seventies the magnetic core memory was replaced by integrated silicon memory. Over the past two decades integrated magnetic has become a reality and with the discovery of the giant magneto-resistance effects in multi-layered film has led to the development of a new type of magnetic memory called magnetic random access memory (MRAM). Although MRAM are more expensive than integrated silicon memory, they are faster and less susceptible to radiation and nonvolatile.

The application of magnetic thin films in integrated devices such as hard disk heads (see above) or novel position or pressure sensors is not trivial. The influence processes, such as annealing, patterning, etching, and packaging have on their properties have only been studied for the past last decade and in particular the influence of stress on the properties of thin magnetic films is currently less understood and for this reason the current process used to integrate magnetic materials in thin film devices will introduce an internal stress to the material, which is difficult to control and can vary largely during device production, hence reducing yield. To combat the problem of uncontrollable stress variation industrial production companies currently avoid the problem by using material's that are less prone to variations in stress sensitivity. A better understanding of the influence of stress on the magnetic properties of thin films would offer designers and production companies more flexibility.

In my thesis work I investigated the influence of stress on magnetic thin films. The work is a continuation of the thesis work of Patrick Holland, who investigated the magneto-elastic properties of thin ferromagnetic NiFe films [13]. Holland et al. measured the hysteresis of thin NiFe samples while applying an isotropic stress to the sample. It was determined that due to this stress the hysteresis decreases significantly [14, 15]. In order to understand his measurement results it is necessary to also know the inverse-magneto-elastic (magnetostriction) properties of the NiFe films. I erected a setup to measure these properties and the measured results of the samples are explained in chapter 5. In addition I also included literary results on the material's properties (Chapter 2 and 3) and how magnetostriction influences the magnetic properties of these films.

CHAPTER 2

SAMPLE PREPARATION PROCESS

Prior to the preparation of the films by a DC Magnetron sputtering process the substrates were cleaned ultrasonically in a 5% micro solution (soap), followed by ultrasonic cleaning in acetone and ultrasonic cleaning in isopropyl alcohol. The substrates were dried with pressurized nitrogen gas. The silicon was covered with a native SiO_2 layer. The substrates were mounted on the substrate holder with metal blade springs and no attempt was made to create a stress free mount during the process. The thin films were sputtered from a NiFe-35% target using a Torus 2C source (sputter pressure=4 mTorr argon with sputter power = 70 W). At these deposition parameters the deposition rate is approximately 3 Å/sec (measured on a thick sample with the stylus profilometer). The film's thickness was estimated from the sputter time and estimated deposition rate and the chemical composition of the samples were checked by Energy Dispersive Spectroscopy (acceleration voltage 15 keV). The iron content of our samples was 31%, which was a little lower than the concentration of the target. A Bede D1 X-ray diffractometer was used to determine the crystal structure of our films. The x-ray data showed a large *FCC* [111] peak in the $2\theta-\theta$ plot so that the texture is the [111] plane [14]. A small [200] peak was observed in the X-ray spectrum, which suggests a 2nd texture exists. Figure 1 below shows the phase diagram for NiFe [18].

The process of coating the substrate was done by a process known as, sputtering and the crystal structure of the films is a non-ordered *FCC*-phase.

Annealing below 517°C results in the chemical ordering of the Ni atoms positioned face centered of an FCC unit cell, while the Fe atoms are positioned at the corners¹.

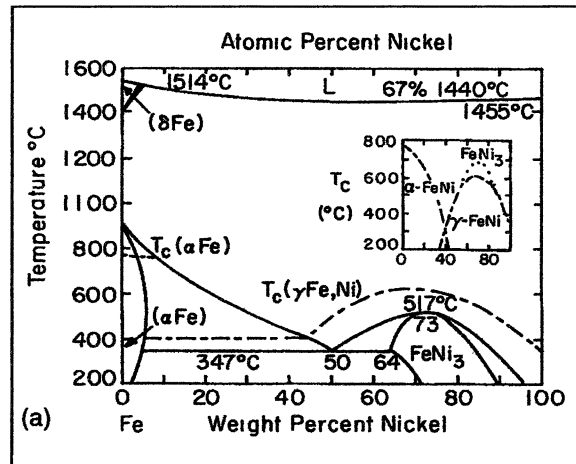


Figure 1: Phase diagram for NiFe system (α is BCC and γ is FCC structure).

Long strips approximately 5 mm by 50 mm were cut from the silicon wafers using a diamond scribe. Not all samples had exactly the same shape and size.

The table below shows the deposition parameters, as well as, the coercivity of a single sample. The coercivity was measured using a Vibrating Sample Magnetometer (VSM) and Kerr Tracer [19].

¹ More details on the sample preparation procedure can be found in [14, 15]

The table below shows the deposition parameters.

Sample ID	Sputter Time (min: sec)	Film Thickness [nm]	Coercivity [Oe]
101601-02	12:31:00	225.3 nm	
101901-01	29:00:00	522 nm	
101901-03	5:33:00	99.9 nm	4.6 (Kerr) 3 (VSM)
101701-03	7:30:00	135 nm	
101901-02	5:33:00	100 nm	
101701-04	7:30:00	135 nm	

Table 1: Data for 31-NiFe on Silicon wafer.

CHAPTER 3

MAGNETIC PROPERTIES

3.1 SATURATION MAGNETIZATION

Ferromagnetic materials are characterized by the fact that the spins of neighboring atoms are aligned in a direction that is parallel to each other. It is the spin of the non-filled states of the electron configuration that is responsible for the creation of a dipole moment and hence the magnetic characteristics. This is very clear if one realizes that filled atomic orbits consist of electrons with opposite spins and thus have no net magnetic dipole moment. For more information on the electronic structure of Ni, Fe, and NiFe see appendix 1. Because of the non-random orientation of the magnetic spins, ferromagnetic objects can have a non-zero magnetic moment in a zero magnetic field. An object will have its maximum magnetic moment if the spins of all atoms are aligned. This will happen when large magnetic fields are applied to the material. The magnetic moment per unit volume at large magnetic field is called the saturation magnetization.

The characteristic properties of the materials magnetization depend on the elemental concentration of chemical composition of which the material is composed. Figure 2 shows the saturation magnetization of NiFe as a function of the chemical concentration nickel.

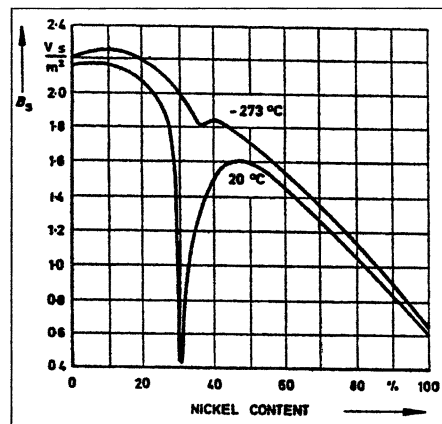


Figure 2: Saturation induction as a function of the nickel concentration for two different temperatures NiFe[16].

The sharp change in the saturation magnetization at 31% nickel content is caused by phase change of the materials characteristic magnetization properties.

The NiFe films investigated in this thesis have an iron concentration of 31% and a Ni concentration of $\sim 69\%$. These samples should have a magnetic induction of 1.25 Vs/m^2 .

Not all ferromagnetic objects have a non-zero ferromagnetic moment. It is possible to demagnetize an iron scissors. In the iron scissors the spins of neighboring atoms are still aligned however one can find different areas in the scissors where the spins have different directions. So the average magnetic moment of the scissors is zero also there is magnetic ordering on the atomistic level. By applying a magnetic field to the scissors it is possible to magnetize it and rotate the directions of the spins in all domains parallel to the field.

The following expression describes the energy of a magnetic material in an external magnetic field:

$$E_{mag} = -\mu_o \vec{H}_{ex} \cdot \vec{M}$$

² Not all ferromagnetic objects have a non-zero ferromagnetic moment

It is clear from this expression that the energy is a minimum when M and H are parallel.

3.2 MAGNETIC ANISOTROPY

The ordered face centered cubic (FCC) crystalline structure for Ni_3Fe is shown in Figure 3 below. The iron atoms are black and situated at the eight corners of the unit cube. The nickel atoms are white and situated on the six faces of the cube. The figure shows one unit cell. The total number of nickel atoms per unit cell is $6 \times 1/2 = 3$ since each nickel atom is shared with a neighbor cell. The total number of iron atoms per unit cell is $8 \times 1/8 = 1$ since each iron atom is shared among eight neighboring cells. The samples investigated in this thesis are not ordered though, so the nickel and iron atoms occupy random sites in the FCC lattice.

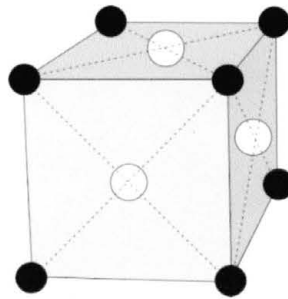


Figure 3: Ordered Ni_3Fe Crystalline Structure (FCC): Iron atoms are black and Nickel atoms are white.

When ordered over a long range the magnetic moments of a symmetric crystalline structure are aligned in a preferred direction with respect to the crystal structure to minimize the internal energy of the system. We call this preferred direction the easy axis. For FCC-nickel the easy axis is the $[111]$ direction. So the energy of the system is lowest if the magnetic moments are aligned in a direction parallel to the diagonal of the unit cell.

While it will take a significant external field to align the spins parallel to any of the three-principle axis of a cubic crystal, those directions are referred to as “hard axis.” For pure iron

that has a body centered cubic structure, the easy axis is along the [100] direction.

The magnetocrystalline anisotropy is the energy needed to deflect the magnetic moments by some angle θ from the easy axis toward the hard axis. For a cubic crystal the magnetocrystalline anisotropy energy is given by a series expansion in terms of the angles between the direction of magnetization and the cube axis, then by series expansion of the anisotropy energy of some arbitrary direction and it is written in terms of the anisotropy coefficient K_1 for NiFe as follows

$$E_a = \frac{K_1}{2} \sum_{p \neq q}^3 \cos(\theta_p) \cos(\theta_q)$$

Here K_1 is a positive constant for NiFe-31 and the easy axis is along [100] so that the θ 's are the angles which the magnetization makes relative to the three crystal axis. The magnetic anisotropy constant is shown below in Figure 4 as a function of nickel concentration for NiFe.

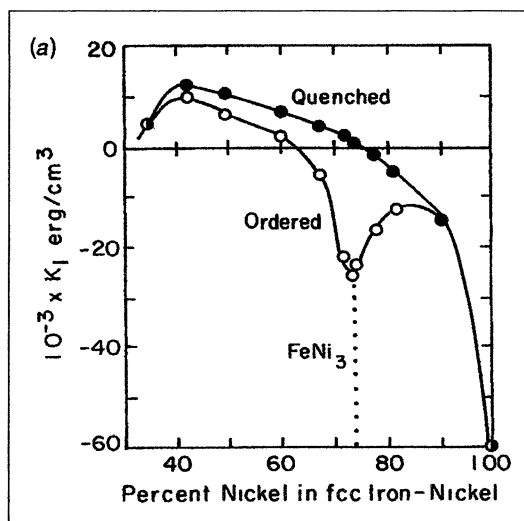


Figure 4: Crystal anisotropy constant as a function of nickel concentration for FCC NiFe.

The thin NiFe films studied in this thesis have a concentration of 31% and therefore the

coefficient K_1 is slightly greater than zero. The samples are polycrystalline and consist of crystals oriented with their [111] plane parallel to the silicon substrate. The easy axis in each crystal is parallel to the [100] direction.

3.3 DEMAGNETIZING FIELDS

Since the crystal anisotropy of our samples is rather small and we only apply a magnetic field in the plane of the sample, it is expected that the magnetic moment will lie in the plane of the film. Assuming the magnetic moment will lie in the plane of the film then the only magnetic poles expected would be at the edges of the sample. Since the films are thin, the magnetic poles are small and the demagnetizing field and energy are negligible. However in the event the external field is applied perpendicular to the film the result is that the top and bottom of the thin film would be covered with magnetic poles leading to a large demagnetizing field.

3.4 MAGNETOSTRICTION

Magnetostriction is a property of ferromagnetic material that will cause a ferromagnetic substance to change its length when acted upon by an external magnetic. A change in length of a substance is often referred to as a strain. The two types of magnetostriction to be considered are the following:

- a. Longitudinal magnetostriction:

$\lambda_L = (\delta r/r)_L \rightarrow$ The change in the length of the material in a direction parallel to the magnetization \vec{M}

- b. Transverse magnetostriction:

$\lambda_T = (\delta r/r)_T \rightarrow$ The change in the length of the material in a direction perpendicular to

the magnetization M .

Because magnetostriction is defined in terms of the change in length of a material, then it is imperative that the two modes of mechanical operandi, one being positive, which elongates the material and the other being negative which contracts the material should be addressed.

This length change can be understood from the perspective of spin-orbit coupling between the spins of nearest neighbor atoms. Not all electron orbitals have the same shape, some are elongated in the XY -plane, and others are extruded in the Z -direction. If there is a strong spin orbit coupling, orienting all the spin of a ferromagnetic material in one direction will likely push the atoms farther apart in the direction of the electron orbits.

Given that there are two different ways to order a ferromagnetic material, it is possible to distinguish two types of magnetostriction:

- a. Spontaneous magnetostriction, which is the ordering of magnetic moments when the temperature is below the Curie point.
- b. Field induced magnetostriction, which is the result from reorientation of domains under influence of an external applied magnetic field.

Figure 5 below shows very clearly the two types of magnetostrictive behavior in terms of domain orientation. The first illustration is the physical state of the magnetic moments when the material is heated above the Curie temperature giving a disordered paramagnetic state. Once the material is cooled below the Curie temperature, magnetic ordering will result in an expansion of the lattice along the direction of magnetization for the material. As the domains are oriented randomly with respect to neighboring domains the size of the sample will increase, hence resulting in a magnetostriction equal to $e/3$, where e is the magnetostriction for a single domain (see Figure 5b). With the application of a magnetic field the material will

expand along the direction of the field at a strain equal to e (see Figure 5c).

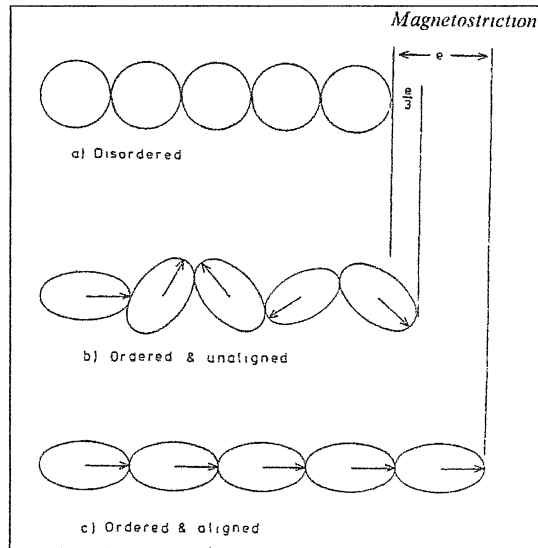


Figure 5: The magnetostriction in (a) disordered (paramagnetic regime); (b) the demagnetized ferromagnetic regime; (c) the magnetized ferromagnetic state (saturation magnetization) [16]

The thin films investigated in this thesis have an overall positive magnetostriction coefficient. Even though the chemical element Ni has a negative coefficient, the value of the chemical elemental composition depends on the Fe concentrations of the sample.

Figure 6 below contains two graphs that show the magnetostriction as a function of the Ni concentration [16]. The left graph shows the magnetostriction coefficients for the quenched and slowly cooled single crystalline NiFe systems. In the right graph, the magnetostriction is shown as a function of the Nickel concentration for the polycrystalline NiFe. If the minimum concentration of 25% Nickel for NiFe is used, then there is a phase transformation of the crystalline structure from $BCC \rightarrow FCC$.

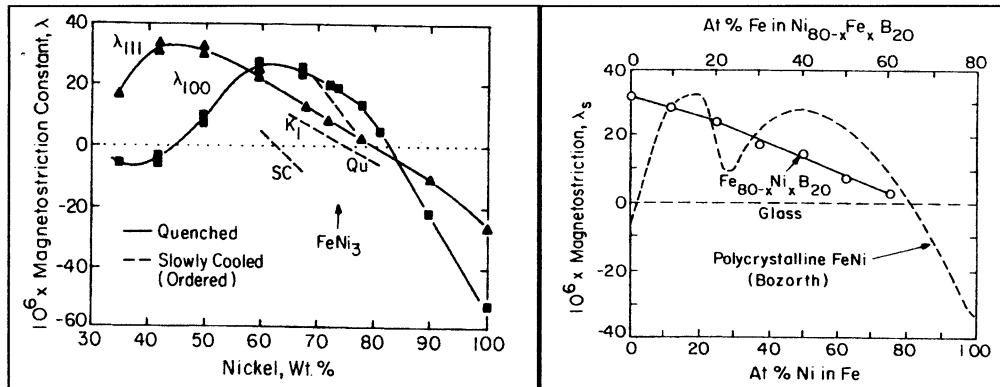


Figure 6: Magnetostriction from single crystalline (left) and polycrystalline NiFe [18]

Given that the magnetostriction relates the reorientation of the spins with the exertion of force, it is clear that the exertion of a force (a strain) on the material will alter the orientation of the magnetization. This effect can be described by a stress dependent crystal anisotropy term [17]:

$$E_{\sigma} = \frac{3}{2} \lambda_{100} \sum_{p,q=m,n}^3 \cos(\theta_p) \cos(\theta_q) \cos(\theta_m) \cos(\theta_n) + \frac{3}{2} \lambda_{100} \sum_{\substack{p=q=m=n \\ p \neq m \neq n}}^3 \cos(\theta_p) \cos(\theta_m) \cos(\theta_q) \cos(\theta_n)$$

Where $\theta_{p,q}$ $p, q \in \{1,2,3\}$ is the angle between the magnetization and the [100] cubic axis, $\theta_{m,n}$ $m, n \in \{1,2,3\}$ is the angle between the stress axis and the [001] cubic axis, σ is the force exerted and E_{λ} is the magnetoelastic energy (the energy associated with magnetostriction)³.

For textured polycrystalline materials one needs to average over the appropriate crystal directions. Since the samples studied in this thesis have a [111] texture the effect of an isotropic in-plane stress is investigated. The magnetostriction of these experimental samples is close to the λ_{111} value of single crystalline material.

³ It should be noted that E_{σ} is only valid for a single crystalline material.

3.5 DOMAIN WALLS

In order to understand the influence of stress on the hysteresis one first should be cognizant of the two types of reversal mechanism in these films:

a. Rotation of the magnetic moment in the domains in a coherent fashion. This type of reversal mechanism is important if the thin film has an in-plane magnetic anisotropy, which would be the case for single crystalline sample. However the unstressed samples used in this experiment are isotropic in the plane.

b. Rather than simultaneously rotating all spin states, the domains that have their magnetic moments oriented parallel to the field will expand at the expense of those whose magnetic moments are oriented anti-parallel to the external field. This reversal mechanism is named domain wall displacement. Domain wall motion happens at relatively low field strengths compared to coherent rotation. Only the atom's residing in the domain walls that have large energy, due to their spin's not being aligned parallel to neighboring atoms.

The 2 types of 180° degree domain wall that exist in ferromagnetic films are as followed:

- a. Bloch walls: The spins rotate in a plane parallel to the domain wall. Such type of domain wall is favorable for bulk materials or thick films. A Bloch domain wall has energy as not all its spins are parallel to each other and not all spins are aligned parallel to the easy axis of the crystal. For films, a demagnetizing term needs to be added to the domain wall energy originating from the magnetic charges at the surfaces of the film. This demagnetizing term is negligible for very thick films.
- b. Neel walls: The spins rotate perpendicular to the domain wall. Such type of domain wall is favorable for very thin films.

The energy expression of a domain wall is given by where

$$\lambda = 2\pi\sqrt{AK}$$

where λ is the energy per unit area, A is the exchange constant, and K the crystal anisotropy constant.

The thickness of the domain wall δ is given by the following expression in terms of the domain wall energy [16].

$$\delta = \frac{\pi\lambda}{2K} \rightarrow \pi\sqrt{\frac{A}{K}}$$

The exchange constant A can be estimated from the Curie temperature T_C of ferromagnetic material [16].

$$A \approx \frac{3k_B T_C}{az}$$

k_B is Boltzmann's constant, T_C is the Curie temperature, a is the lattice parameter, and z is the number of nearest neighbors.

The graph in Figure 7 shows the Curie temperature (and other parameters) as a function of the nickel concentration for the NiFe system.

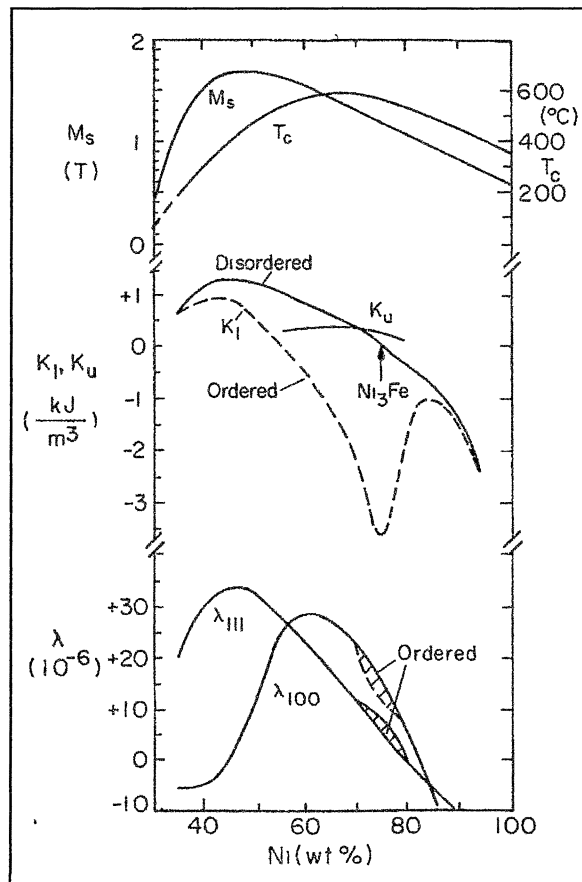


Figure 7: Curie temperature as a function of Nickel concentration.

The magnetization reversal in thin film is mainly due to domain wall motion as shown by Ten, Brinke and Sombroek [19]. The Figure 8 shows the domain pattern oriented in the direction of a small external magnetic field for a 31% NiFe film.

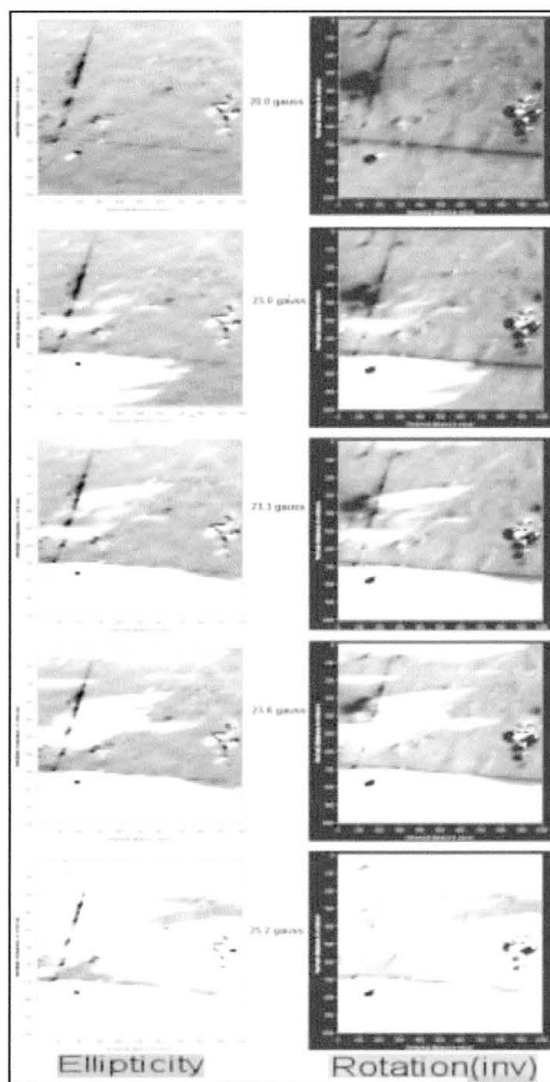


Figure 8: Kerr effects grey to right magnetic moments and white to the left.

Other properties of the resistance and magnetoresistance of the NiFe film that are not relevant to the magnetoelastic properties are included in Appendix 1.

CHAPTER 4

THE EFFECT OF STRESS ON THE MAGNETIC HYSTERESIS

In a uniform ferromagnetic sample there exist regions of discontinuity of the magnetization normal components across the boundaries, creating fields that raise the energy level associated with the system. The creation of domains decreases the energy associated with these discontinuities at the price of the domain wall energy.

The effect of stress on a ferromagnetic sample can influence the magnetic hysteresis properties in several different ways:

- a. The magnetostriction stress can change the magnetic anisotropy and therefore affect the field necessary to rotate the magnetic moment in a system of N -domains. The best way to understand what is happening is to combine the anisotropy energy and magneto-elastic energy terms as given in chapter 3. As an isotropic in-plane stress is applied to the samples, there is no easy axis induced in the sample plane due to stress. However the unstressed 31% NiFe will have an easy axis in the $[100]$ direction. The figure below shows that the $[100]$ directions are slightly out of the plane of the sample.

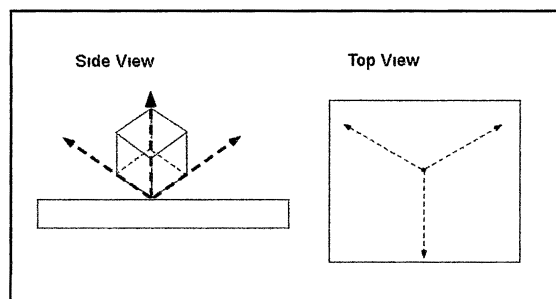


Figure 9: Easy axis along the [100] plane for NiFe-31

Assuming the easy axis angle is 55 degrees with respect to the normal plane of the film, then the demagnetizing energy and crystal anisotropy energy ratio compare as follows:

$$0.5\mu_0(M_s \cos(55)) \leftrightarrow K_1$$

and

$$4.9 \text{ kJ/m}^3 \leftrightarrow 0.39 \text{ kJ/m}^3$$

The film is therefore magnetized parallel to the substrate.

The above ratio is a comparison between the shape anisotropy and the crystal anisotropy energy. Referring to Figure 7 and the graph at the top of the Figure, M_s as a function of Nickel concentration, because the demagnetizing energy is much larger than the crystal anisotropy energy, the magnetic spin moments are oriented parallel to the plane of the film. To align the magnetic moments (i.e. magnetization) in the easy direction, i.e. 35 degrees out of the substrate plane, the amount of energy needed would be 4.9 kJ/m^3 at a gain of 0.35 kJ/m^3 .

Since the magnetostriction is positive we expect the difference between the ratio of demagnetizing and anisotropy energies will be larger when the tensile stress is in the plane of the film.

b. The magnetostriction stress can change the magnetic anisotropy and therefore affect the

domain wall energy in the thin film.

The domains of a ferromagnetic sample are aligned as a spontaneous geometric set of favorable orientation parallel to the easy axis. At the boundary of neighboring domains there exist regions where the spins of neighboring atoms are not aligned parallel to each other, the formation of domain wall is the result minimizing the demagnetization effect (dipolar magnetic fields) of anti-parallel spin moments (see Chapter 3). If a field is applied to the material the domains that are aligned parallel to the field will grow at the expense of those aligned anti-parallel and orthogonal to the fields. The result is that those domains aligned in the direction of the field will grow in development while those that are not aligned to that of the field will constrict. The overall effect is the displacement of the area where the spins are not parallel to each other, i.e. the domain wall.

The displacement of domain walls is not constant as a function of the position and varies throughout the sample volume. This variation of the domain wall energy serves as the basis for impeding or restricting the domain wall motion.

The variation of the domain wall energy with the position can be caused by several mechanisms:

- a. The stress in the thin film can vary as a function of the position. This is very plausible for polycrystalline thin films as explained in chapter 3, but also due to lattice defects caused by impurities or grain boundaries, which cause variations of localized stress. Such stress variations will lead to a variation of the effective anisotropy constant, $K_1 \rightarrow K_{eff}$ and thus lead to changes in wall energy.

Case in point, let the stress vary according to $\sigma = \sigma_o(1 - \cos(2\pi x/l))$ where x is the displacement of the 180° wall, l is the periodicity of stress and σ_o is the maximum

amplitude of the stress variation. In a magnetic field the total energy of the system is given by two terms, the magnetoelastic energy and the magnetostatic energy:

$$E_{tot} = E_{me} + E_{ms} = \frac{3}{2} \lambda \sigma_o (1 - \cos(2\pi x/l)) - 2\mu_o M_s H x$$

Expanding $\cos(2\pi x/l)$ in terms of Taylor expansion and letting

$E_{tot} = 0$ (equilibrium) implies:

$$6\lambda\sigma_o \left[\frac{\pi^2 x^2}{l^2} \right] - 2\mu_o M_s H x = 0$$

and

$$x = \frac{l^2 \mu_o M_s H}{3\pi^2 \lambda \sigma_o}$$

So the position of the domain wall changes for higher values of the magnetic field H .

The solution parameter x is a measure of the distance between the defects, called pinning sites. The smaller this parameter is the more difficult it is to move the domain wall through the material and thus the larger the coercivity. The parameter σ_o depends on the type of defects but maybe also depend on the strain of the layer: if the atoms are farther apart then normally, it is likely that an impurity atom, interstitial, will have more space and create a smaller localized strain. This idea is illustrated in the figure below.

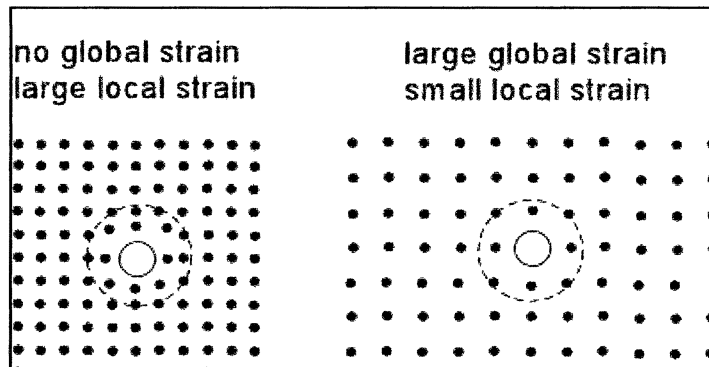


Figure 10: Localized and Global Strain.

- b. The thin film can consist of two different phases. If both phases have different magnetic properties, the domain wall will be pinned at regions of in-homogeneity. The 2 important effects are: (1) domain wall energy of both and (2) the saturation magnetization.
- c. The domain wall energy can vary as a function of position in the presence of grains with different crystal orientation. In particular when the crystal size is significantly larger than the domain wall width, large effects are to be expected. Since all the samples investigated in this thesis are optically smooth, we do not expect the crystal size to be larger than 300 nm. In the thin film sputter deposition process the size of the crystallites are often smaller than the film thickness.

CHAPTER 5

MAGNETOSTRICTION SETUP

5.1 PRINCIPLE OF THE SETUP

The magnetostriction setup is an arrangement of electronic equipment, software and hardware mounted on a non-magnetic optically damped table to reduce any ambient noise and or vibration during the experimental measurement process.

The sample is a rectangular beam of 4 mm by 40+ mm that is constricted on one side and placed at the center of the Helmholtz coils. Two orthogonal sets of Helmholtz coils are used to apply a rotating magnetic field to the sample. The field is directed into the plane of the sample. If the sample has a non-zero magnetostriction, the sample will vibrate with twice the angular frequency of that of the rotating magnetic field.

To measure the displacement of the sample when a magnetic field is applied an optical sensor is placed normal to the plane of the rectangular sample. The optical sensor is mounted on a platform that allows the user to adjust the distance between the sample and the optical probe to allow for a true relative displacement of sample probe distance to optimize sensitivity.

Assuming that the sample is a thin parallelogram (with positive magnetostriction) of length L and width W on a silicon substrate then the expectation of its deformation behavior is as follows:

When the magnetic field is parallel to L at some time t the sample's strained state will be elongated in the direction of the field and bend in the direction opposite to that of the optical sensor. (Note that the silicon substrate is not influenced by the magnetic field).

At a time $t + \Delta t$ when the magnetic field is parallel to W the sample will elongate in the direction of the applied field and contract in the direction parallel to L . The sample will bend in the direction towards the sensor.

In the following sections the different parts of the setup are discussed in detail.

5.2 DEFLECTION COEFFICIENT

The mechanical behavior of the film is the result of the transition from the ordered-disordered state of an isotropic ferromagnetic film on a non-magnetic substrate. The transitional state (rotation of the magnetization) arises from an externally applied field that is parallel to the plane of the ferromagnetic sample.

As mentioned earlier the volume of the material has to be preserved during deformation, which implies that any change to the ferromagnetic material length would result in a change about the axis orthogonal to the ensuing axis. For instance if the material being examined has a positive magnetostriction, then the plane orthogonal to the elongated axis would contract such that its volume would be preserved and vice versa for negative magnetostriction. The process of computing the deformation coefficient is based on the thickness of the film, substrate and the overall geometry of the sample. If χ is the stiffness ratio of film to substrate and ζ is the thickness ratio of film to substrate, then it can be shown that

$$\chi = \frac{E_{film} (1 - \nu_{film}^2)}{E_{substrate} (1 - \nu_{substrate}^2)}$$

and

$$\zeta = \frac{t_{film}}{t_{substrate}}$$

In this expression the dimensionless parameters associated with the deformation coefficient are defined as Young's modulus $E_{Film,Substrate}$ and Poisson's ratio $\nu_{Film,Substrate}$.

Given that any geometric structure the volume is assumed preserved for any change from its initial geometric state to that which mimics that of a cantilever (Figure 11 b),

The action of the applied field will result in a bi-directional field due to the physical makeup of the system of Helmholtz Coils. Because the coils are in an orthogonal coordinate frame the action of the external field will result in a concave shape of the surface of the film when the field is in the direction opposite the longest dimensions and yet parallel to the plane of the sample. The remaining field direction is parallel to the plane of the sample's longitudinal plane whose geometric surface resembles that of a convex plane. [1]

Because the geometry of the sample is a function of the magnetostriction it is essential that the mechanical characteristics (deflection coefficient) be computed.

Assuming the stress of the sample is along the longitudinal axis of the rectangular sample then $\epsilon_{(x,y),(film,substrate)}$ represents the difference between the total strain and expansion of the sample. Therefore the net magnetization is in the direction of the longitudinal axis and hence the strain of the ferromagnetic film and substrate is defined in terms of the strain of the film and that of the substrate itself.

Because the magnetic induction field setup is bi-directional to the surface plane of the sample and choosing the z-axis as normal to the sample, then there exists a strain state in the direction normal to the surface of the rectangular plane.

$$\sigma_{y,substrate} = - \left[\frac{E_{substrate}}{1 - \nu_{substrate}^2} \right] (\epsilon_{y,substrate} + \nu_{substrate} \epsilon_{x,substrate})$$

$$\sigma_{y, film} = -\frac{E_{film}}{1-\nu_{film}^2} \left((\varepsilon_{y, film} - \lambda_{saturation}) + \nu_{film} (\varepsilon_{x, film} + \lambda_{saturation} / 2) \right)$$

and

$$\sigma_{x, film} = -\frac{E_{film}}{1-\nu_{film}^2} \left((\varepsilon_{x, film} - \lambda_{saturation}) + \nu_{film} (\varepsilon_{y, film} - \lambda_{saturation} / 2) \right)$$

The strain state is defined in terms of the radii of curvature of the sample with respect to the mid-point ε_{x_0, y_0} as $\varepsilon_{(x,y), p} = \varepsilon_{x_0, y_0} - z/R_{x,y}$ where p is the subscript for film and substrate.

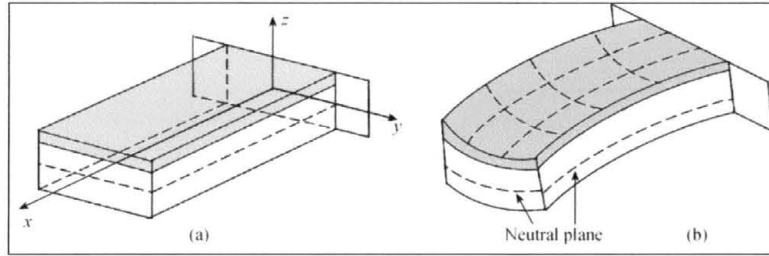


Figure 11: (a) Rectangular sample unstrained state (b) Strain state of rectangular sample.

The experimental magnetostriction measurement setup for saturation of the ferromagnetic sample is such that the magnetic film is fixed at one end. When the sample reaches a state where the magnetic moment are aligned parallel to the field defined as the ordered strain state then

$$\int \sigma_{x, film} dydz + \int \sigma_{x, substrate} dydz = 0, \quad \int \sigma_{y, film} dx dz + \int \sigma_{y, substrate} dx dz = 0$$

and

$$\int \sigma_{x, film} z dydz + \int \sigma_{x, substrate} z dydz = 0 \quad \int \sigma_{y, film} z dx dz + \int \sigma_{y, substrate} z dx dz = 0$$

Solving the analytical solution for the set of linear equations implies [16]

$$\alpha_{x,y} = -\frac{3}{2} \chi k (k+1) \left[(1+\nu_f)(1+\nu_s)A + 3(1-\nu_f)(1-\nu_s)B \right]$$

Let D define the deflection function of a rectangular sample and let A and B be the coefficients associated with the parameters of the film and substrate

$$D = -\frac{3\chi k(k+1)L^2}{4t_{substrate}} \left[(1+\nu_f)(1+\nu_s)A + 3(1-\nu_f)(1-\nu_s)B \right]$$

When $t_{substrate} \gg t_{film}$, the deflection coefficient is as follows

$$D = \frac{3L^2 t_{film} \lambda_{saturation}}{2t_{substrate}^2} \frac{E_{film}}{E_{substrate}} \frac{(2(1-\nu_{film}\nu_{substrate}) - (\nu_{film} - \nu_{substrate}))}{(1-\nu_{film}^2)}$$

These mathematical computations show that the surface area element of a thin ferromagnetic sample is not preserved under the action of an external field and the deformation of the film, whether for positive or negative magnetostriction, will result in a change in the overall geometry with respect to the longitudinal axis and the axis normal to the longitudinal plane of the sample. Hence there exist two directions in which the deflection coefficient is measured, $D_{||}$ and D_{\perp} [1] [16].

5.3 SAMPLE HOLDER

The sample holder is used to isolate the ferromagnetic thin film so that its plane initially is normal to the direction of the optical probe. It is crucial that the sample remain isolated as the cantilever propagates back and forth when the sample is acted upon by an external magnetic field [8].

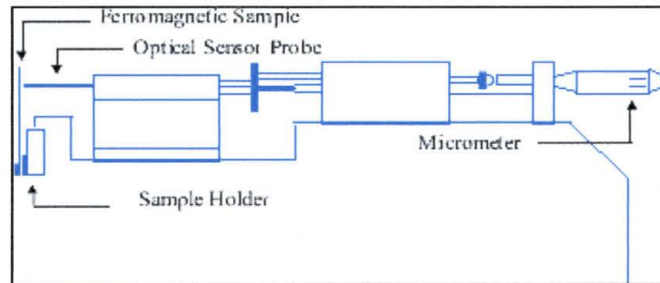


Figure 12: Optical Sensor and Sample Holder Setup.

5.4 FOTONIC SENSOR



Figure 13: The front face of the MT-2000 Fotonic Sensor.

To measure the displacement of the sample when a magnetic field is applied an optical sensor (with 2.5 \AA resolution) is placed normal to the plane of the rectangular surface of the sample. The optical sensor is mounted on a platform that allows the user to adjust the distance between the sample and the optical probe to allow maximum displacement sensitivity.

The optical probe tip is made up of uniformly placed transmission and reflection light fibers, which increase the displacement sensitivity of the probe for short-range measurements. The probe module is a 0.00590 um/mV optical probe. The module consists of a set of two types of optical fibers. The first set of optical fibers is connected to a light source, while the 2nd set of optical fibers is connected to a detector. The optical coupling between both sets of fibers depends on the sample to optical probe distance. If the sample probe distance is infinite

(i.e. there is no sample mounted in place) then the amount of light measured by the detector will be zero. If a reflecting is placed close to the probe, part of the light emitted from fibers connected to the light source will be reflected back to the fibers connected to the detector.

Figure 14 is an illustration of the range of the target-sample to probe displacement for optimal measured experimental results. It is clear from the graph of Figure 15 that there exist a range over which the measured intensity is a very steep linear function of the probe to target displacement (probe gap). To achieve maximal intensity the target sample is placed closely to the optical probe in the region defined as range 1.

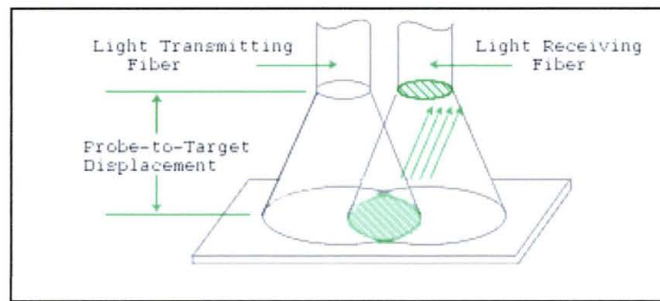


Figure 14: The Probe to-Target Displacement of the receiving and transmitting optical fibers in relation to the plane of the sample.

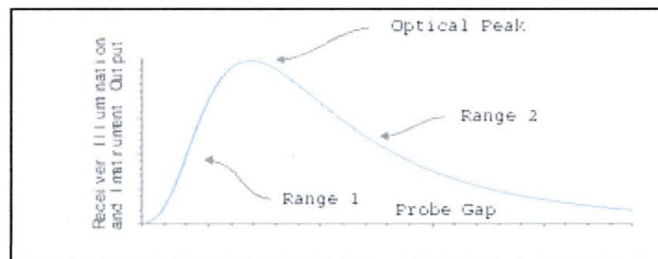


Figure 15: Maximum Optical peak for distance of optical device to film sample.

Calibration of the photonic sensor is a necessity of the experimental measurement step for each sequential set of measured data. To calibrate the photonic sensor, first position the offset switches in the down position located on the rear panel.

Turn the light switch to the on position.

Place the mode switch in the “Cal” position. This prevents the instrument from being saturated while the operator adjusts the dial, located at the opposite end of the probe, to find the optical peak. A display bar graph located on the front panel of the sensor will indicate the proximity of the probe to sample distance, which should be as close as possible without making contact with each other.

Depress and release the Calibration Set-point Switch, which activates the Auto Calibration sequence.

Maximize the linear operating range of the probe by adjusting the position of the probe such that it is moving forward toward the sample until the digital meter indicator reading is zero.

For this particular experiment it is important that during the experimental process the maximum sensitivity is maintained, to minimize the error of the measured results. It is understood that during the course of experimental measurement of the sample displacement that there exists a minimal displacement from the plane of the target sample to optical sensor, which defines the optimum peak value to minimize the error of the measured displacement. It is important that the system is recalibrated each time a new sample is loaded.

5.5 MAGNETIC FIELD VECTOR OF HELMHOLTZ COILS

The set of Helmholtz Coils consists of two independent sets of copper wire spools. The set of coils are positioned at an angle of $\pi/2$ radians with respect to one another. The

importance of the sample's position relative to the midpoint of the two set of coils is such that it gets exposed to a uniform rotating magnetic field. The slight displacement of the sample should not result in the sample being exposed to a significant different magnetic field.

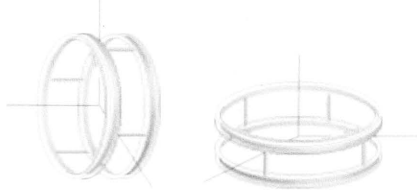


Figure 16: The Inner and Outer Helmholtz Coils, deconstructed.

The magnetic field lines of a single set of coils of N -loops, the field is greatest at a region about the center of the coil.

$$H = \frac{INa^2, b^2}{2(a^2, b^2 + (z, x \pm L/2)^2)^{3/2}} \hat{k}, \hat{j}$$

Let $z \ll a, b$ and $z < L/2$, then the magnetic field of the set of coils is as follows:

$$H = \frac{IN}{2a, b(1 + (z, x \pm L/2)^2 / (a, b)^2)^{3/2}} \hat{k}, \hat{j}$$

Because the point of interest is the magnitude of the induction field H with respect to a localized region then expanding equation such

that $f(z, x) = (1 + ((z, x \pm L/2)/a, b)^2)^{-3/2}$ implies:

$$df(z, x) = -3(1 + ((z, x \pm L/2)/a, b)^2)^{-5/2} ((z, x \pm L/2)/a^2, b^2)$$

and

$$d^2 f(z, x) = -3(1 + ((z, x \pm L/2)/a, b)^2)^{-5/2} / a^2, b^2 + 15((z, x \pm L/2)/a^2, b^2)^2 (1 + ((z, x \pm L/2)/a, b)^2)^{-7/2}$$

Computing the magnetic field components of the two Helmholtz Coils (the variable “ c ” is the constant $NI \ni I = I_0 e^{\pm i\omega t}$).

$$H_k = c \left(I + \left(\frac{z \pm L/2}{a} \right)^2 \right)^{-3/2} - 3c(z - z_0) \left(I + \left(\frac{z \pm L/2}{a} \right)^2 \right)^{-5/2} \left[\frac{z \pm L/2}{a^2} \right] \\ - c \frac{(z - z_0) \left(I + \left(\frac{z \pm L/2}{a} \right)^2 \right)^{-5/2}}{2a^2} + c \frac{15 \left(\frac{z \pm L/2}{a} \right)^2}{2} \left(I + \left(\frac{z \pm L/2}{a} \right)^2 \right)^{-7/2}$$

and

$$H_j = c \left(I + \left(\frac{x \pm L/2}{b} \right)^2 \right)^{-3/2} - 3c(x - x_0) \left(I + \left(\frac{x \pm L/2}{b} \right)^2 \right)^{-5/2} \left[\frac{x \pm L/2}{b^2} \right] \\ - c \frac{(x - x_0) \left(I + \left(\frac{x \pm L/2}{b} \right)^2 \right)^{-5/2}}{2b^2} + c \frac{15 \left(\frac{x \pm L/2}{b} \right)^2}{2} \left(I + \left(\frac{x \pm L/2}{b} \right)^2 \right)^{-7/2}$$

The variable “ z ” is the variable which represents the axial field of the Inner coils of radius “ a ,” while the variable “ x ” is the variable which represents the axial field of the Outer coils of radius “ b .”

The purpose of this particular approach to computing the magnetic field induction is that it provides a very accurate measurement of the fields for both the Inner and Outer coil for a small region about the origin where the fields emanating from the set of coils converge.

5.6 AC POWER SUPPLY OF THE HELMHOLTZ COIL SETUP

A *Carver Magnetic Field Amplifier model M-1.0t*, which is a 350-watt per channel audio amplifier, is used as an AC power source for the Helmholtz coil set. The amplifier, which consists of two output ports, one for each set of Helmholtz Coils, is used to increase the amplitude of the initial field created by the control software and DAQ card. The signal from the DAQ card is sent to two independent input ports located on the rear panel of the power amplifier. The maximum current that can be provided by the amplifier is approximately

4 Amperes, which is sufficient for a field of 30 Oersted.



Figure 17: The front and back panel of the Carver MT1.0T Magnetic Amplifier.

5.7 JUNCTION BOX

To limit the amount of current to the coils a series of electrical components, including a power resistor and fuse for each set of coils, is installed in a rectangular box that precedes the signal to the Helmholtz Coils. The Junction box, in addition to being a current limiter, also serves as a node for the SCB-68 DAQ Board.

	Inner Input	Outer Input
Resistor (Ohms)	1.799	2.789
Fuse (Ampere)	4.0	4.0

Table 2: Electrical properties of components inside Junction Box.

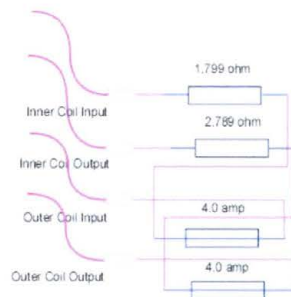


Figure 18: The electrical hardware between the Carver MT1.0T Magnetic amplifier and the system of Helmholtz coils.

5.8 DATA ACQUISITION BOARD (DAQ)

The *SCB-68* interface board supplied by National Instruments, interacts with the *NI-6040E DAQ card* to transmit and receive signals from the experimental hardware and Lab-View software. The DAQ card includes all the basic algorithms associated with the analog inputs and outputs, digital inputs and outputs, and counter/timer.

The wiring schematic for the interface board are as follows:

Two sinusoidal signals generated by the control software are sent to the DAQ (Data Acquisition Board) where the signal is converted from a digital to an analog signal for channels 0 and 1; the analog signals are fed into the inputs of the Carver amplifier; the outputs of the Carver amplifier are connected to both the *Inner and Outer Coils*.

The voltage signal across the series resistors in the Junction Box are connected to input channels 0 and 1 of the DAQ. The signals are converted from analogue to digital by the DAQ and used by the Lab-View software to monitor the current through the coils. Both signals can be displayed by the software, so the user can monitor the phase shift between them.

In addition to the signal received and transmitted by the coils, the DAQ card serves as an interface for the signal transmitted by the optical probe. The analogue output of the optical probe is connected to channel 2 of the DAQ card.

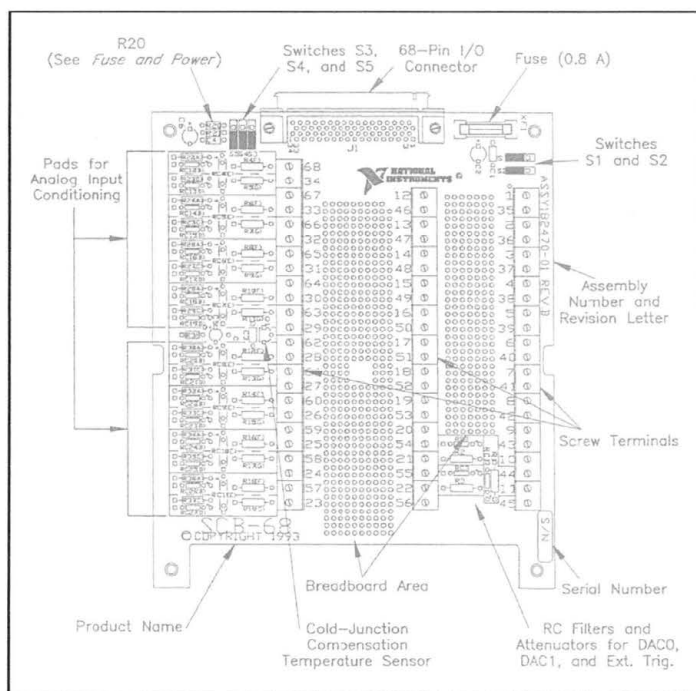


Figure 19: An illustration of the breadboard, which serves as an electrical contact between the National Instruments PCI-GPIB board and the external hardware.

The data acquired by the general-purpose interface board uses a process known as sampling. The sampling of an analog signal involves taking a set signal at a discrete time. This rate at which the signal is sampled is known as *sampling frequency*. The minimum sampling frequency required to represent the signal should at least be *twice the maximum frequency* of the analog signal. The measured sample oscillates with twice the angular frequency of the driving magnetic field therefore the sample frequency must be set at a value that twice the frequency.

used by the “Sinc” program.

Once the signal is set it is converted from an analog to digital signal for all three channels. The analog to digital code converts the signal to a set of numerical digits ranging from 0 to 1 and in turn is further scaled by the algorithm.

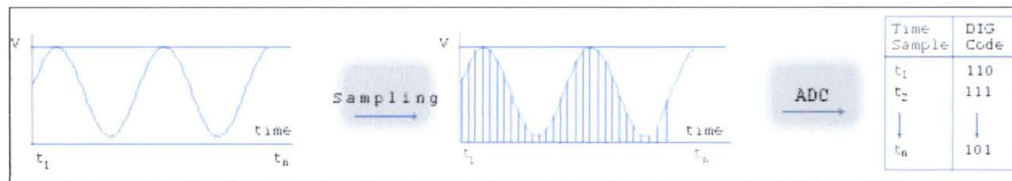


Figure 20: Analog to Digital conversion process for the PCI-GPIB Board.

5.9 OSCILLOSCOPE

To monitor the signal of the position sensor the analog output of the Fotonix Sensor is monitored on an oscilloscope screen. The monitoring instrument is a *Tektronix 2467B* Oscilloscope. This enables the monitoring and detection of sound vibrations during the measured experimental process.

5.10 CONTROL SOFTWARE: LAB-VIEW PROGRAM

The heart of the Lab-View program is the main program titled “DIRECT MAGNETOSTRICTION.” The program is a sequence of object-oriented tasks designed to measure the strength of the magnetic field emanating from the Helmholtz coils, the deflection of the ferromagnetic thin film when perturbed by an external magnetic field and the magnetostriction coefficient of the target sample.

At the beginning of the program is a set of operations that must first be executed before the actual measurement program can start. One task is to load a list of tabulated and sample

information and measured parameters, which are stored in a text file (Young's modulus, film and substrate thickness, sensor clamp distance, length of the target sample and standard chronological information).

The sensor clamp distance is a constant coefficient that does not change even if the geometry of the film does. It is however an important entity in the experimental process. In Figure 21 is a diagram of the program "DIRECT MAGNETOSTRICTION." The 1st figure is the source code for "Direct Magnetostriction" program, while the illustration below Figure 22 is the graphical user interface (GUI) which contains the sample information, user and developer controls.

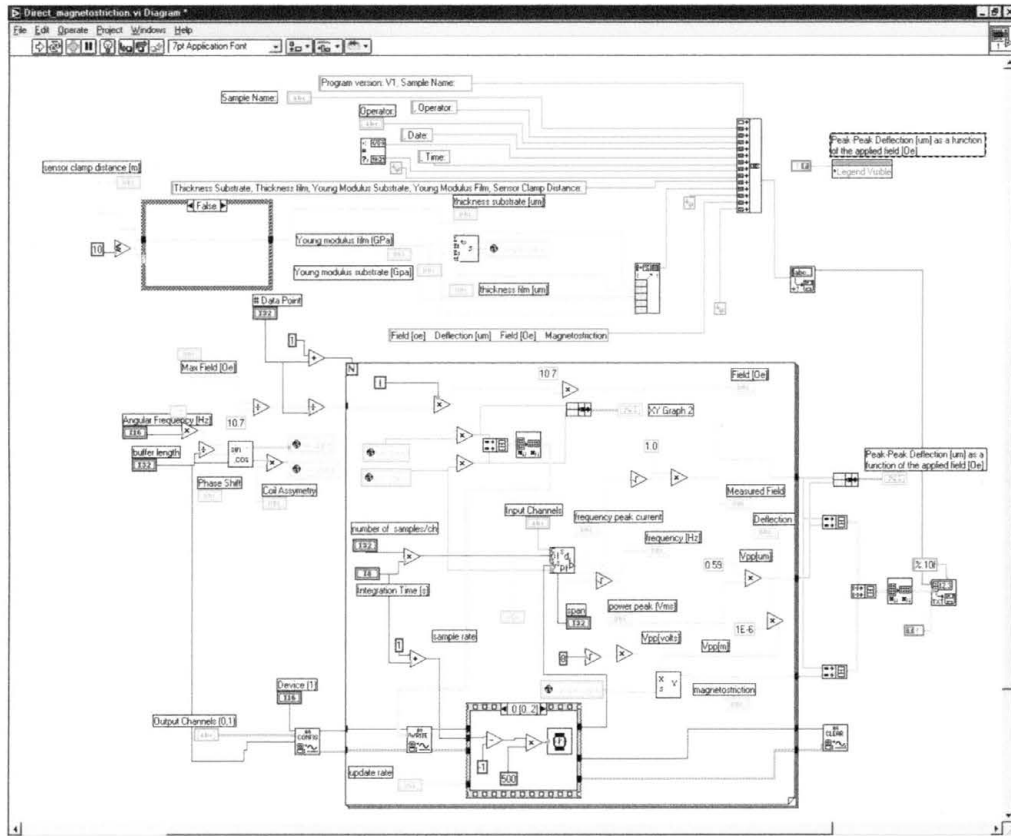


Figure 21: Source code for the program “Direct Magnetostriction.”

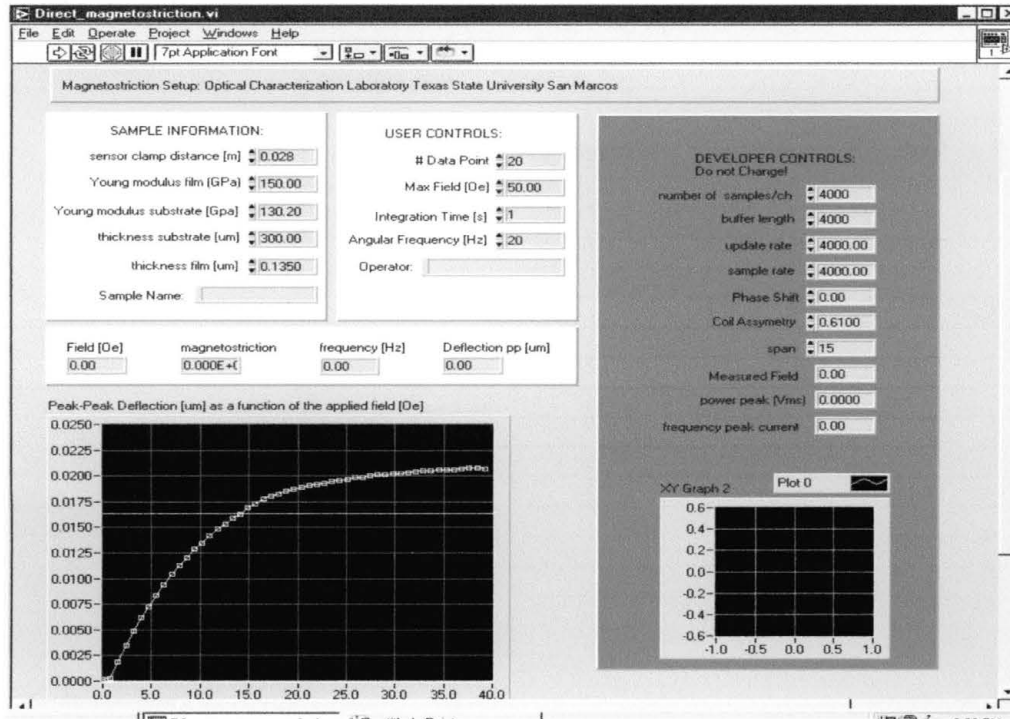


Figure 22: The main Lab-View VI Program to measure the Magnetostriction and Deflection coefficient as a function of time dependent Magnetic Induction fields.

The sinusoidal signal that is received by the coils is computed by the subprogram SIN-COS. The program computes two independent sinusoidal signals that are used to create a time dependent signal in both the inner and outer Helmholtz Coils. The signals created by the subprogram differ in phase by $\pi/2$ radians with respect to one another and each signal is loaded in an array with a buffer length (temporary storage) of 4000-elements. The array is a sequence of numerical elements, which appear in several aspects of the algorithmic process by defining it as a “Global” variable.

The mediator, which serves as a communication device between the hardware and software is the DAQ card (architectural library of object-oriented task), which is manufactured by National Instruments. The DAQ is a compilation of electronic solid-state devices designed

to interpret and transmit information from the experimental hardware and the Lab-view “VI” programs. The DAQ’s Data Acquisition main task is to acquire and transmit data to the Central processing unit.

In the figure below is a portion of the “DIRECT MAGNETOSTRICTION” program that is used to configure the task of Analog Signal Output. The VI calls several advanced analog output VI’s to set up the task for a buffered analog output. The *Analog Output Configuration VI* calls the ‘*Analog Output Group Configure*’ VI for the specified device number, group of channels or grouped channels to create an identification task (ID). The task ID is used to call other advanced analog output VI’s to set up a task for a buffered analog output, which all the analog output VI’s use. The *Analog Output Configure VI* then calls the *AO Hardware Configure VI*, which configures the peak-to-peak voltage, output polarity and the unit (a single quantity regarded as a whole) of measured data obtained for the specified channels. The *AO Hardware Configure VI* expedites the current settings for all the channels in the specified group to record information about the hardware configuration. The *AO Configure VI* then calls the Analog Output Buffer Configure VI to allocate memory for the analog output buffer. The *Analog Output Buffer* is a set of stored data for channels “0” and “1” and assigns the channels to a group by calling a variable that can be accessed by all parts of a program.

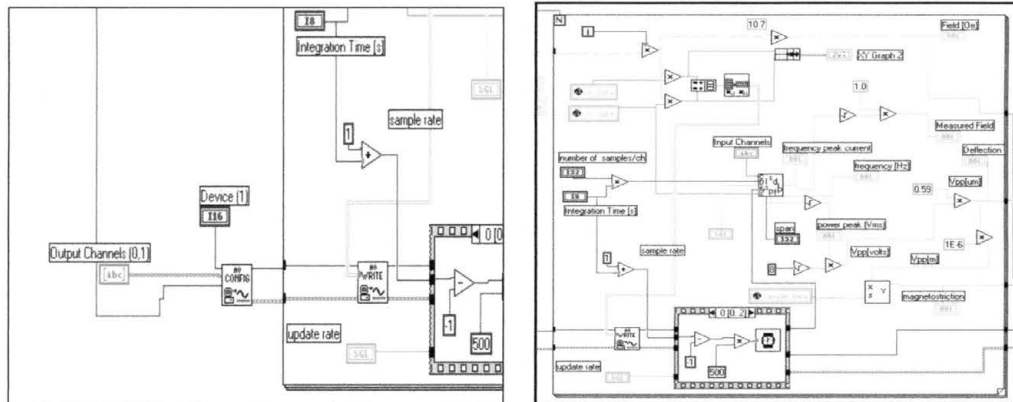


Figure 23: The "Magnetostriction" Lab-View VI Program to measure the Magnetostriction and Deflection coefficient as a function of time dependent Magnetic Induction field.

At the center of the "Direct Magnetostriction" program is a code defined as "For Loop." The "For Loop" initiates at set of operations that are contained inside its perimeter for an assigned number of N-iterative steps. The operations within the perimeter of the "For Loop" are a set of operations, which make it possible to compute the experimental data (oscillating amplitude, deflection coefficient, D and the magnetostriction coefficient, λ) for each iterative step.

The signal for the Helmholtz Coils is calculated in the upper left portion of the "for loop" of the *Magnetostriction program* and its data is stored as a two dimensional array. The *Analog Output Write VI* or "AO Write," writes the data from the global variables "Sin Data" and "Cos Data" into the buffer for a buffered analog output operation. The global data, prior to being stored in the buffer is composed of a set of a transposed 4000 by 2 matrix. (Note that 4000 is the buffer length and there are two rows, one for the sine signal and one for the cosine signal). Yet before the process of computing the experimental coefficients certain precautionary measurements have been instated to prevent any thermal instability from interfering with the signal, noise, as well

as, to ensure that any increase in temperature due to current does not exceed the maximum current set by the physical parameters of the coils and causing a thermal break down.

To implement the precautionary process a sequence of structures has been placed within the perimeter of the “*while loop*.” The structure is an object orientated set of sequential task that contain a set of subprograms. The first structure is a time-based operation, which is determined by the user. The timed based operation is one that is a period of 500 milliseconds, which is initiated before the signal sent from the coils is allowed to proceed (time delay process).

The 2nd sequential operation is the *Analog Output Start VI*, which calls the *AO Clock Configure VI* task ID for group “0” and the I/O operation to configure the output operation using a Time-based VI at an update rate of 4000 updates/second .

The total number of periods the buffered I/O sends to the digital to analog is equal to the integration period of a *1 second*, which means that the current flowing through the Helmholtz Coils will only last for a period not to exceed the integration period of a single second.

The 3rd and final sequential operation is one in which a period of 200 millisecond between each N-iterative operation to insure that the transient part of the vibration associated with the initial start of the signal through the coils is damped out before the accumulation of data is allowed to proceed.

Because the magnetic field is only present for an integration period of *1 second*, as well as, the 200 millisecond period before initial data is taken, the field is only present during the period needed to accumulate the pre-determined amount of data, thus the field is only present for a period of no more than that of the integration time.

WAAR is a subprogram in which the *Multi Analog Input VI* acquires the data from

channels “0” and “1” and samples the channels at a scan rate of 4000 scans/second. The VI performs a timed measurement of the multiple input waveforms based on the *Analog Clock Configuration VI*.

The output of the *Multi Analog Input VI* is a 2-dimensional array that contains analog input data in scaled units specified by the programmer. The array is a column of numerical values for each individual channel. The first two columns are the current data for both the *Inner and Outer Helmholtz Coils*. The 3rd column is the deflection of the ferromagnetic sample for each sequential set of operations.

To better understand the complexities of the operations recently discussed is a plot of the sub-program “WAAR” as well as the modular panel display is provided below.

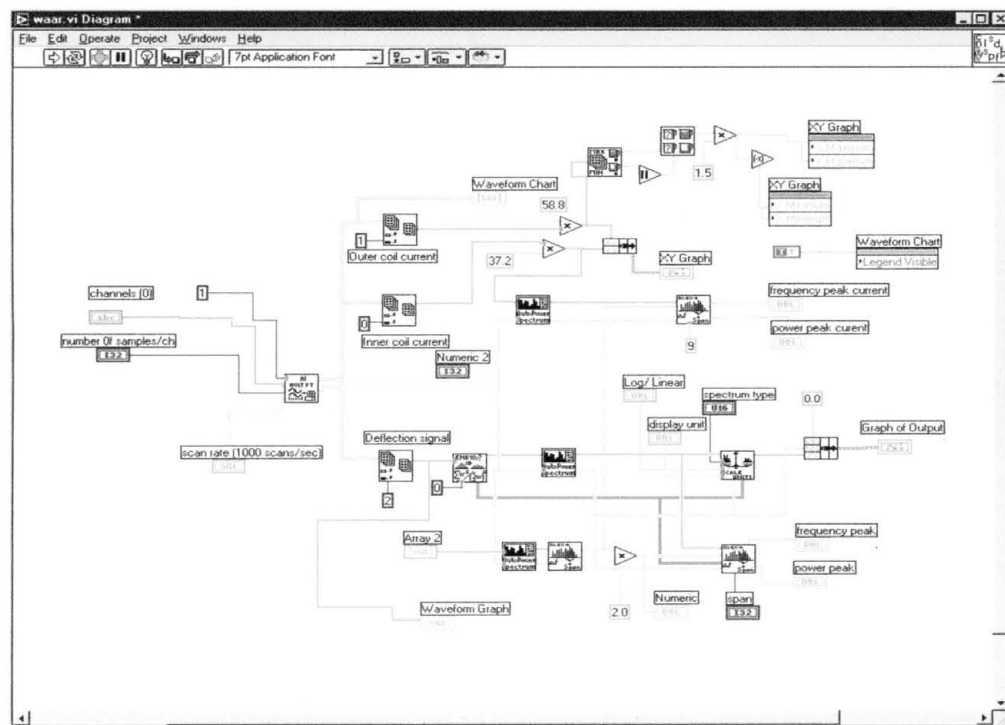


Figure 24: The Object Oriented VI Program “WAAR.”

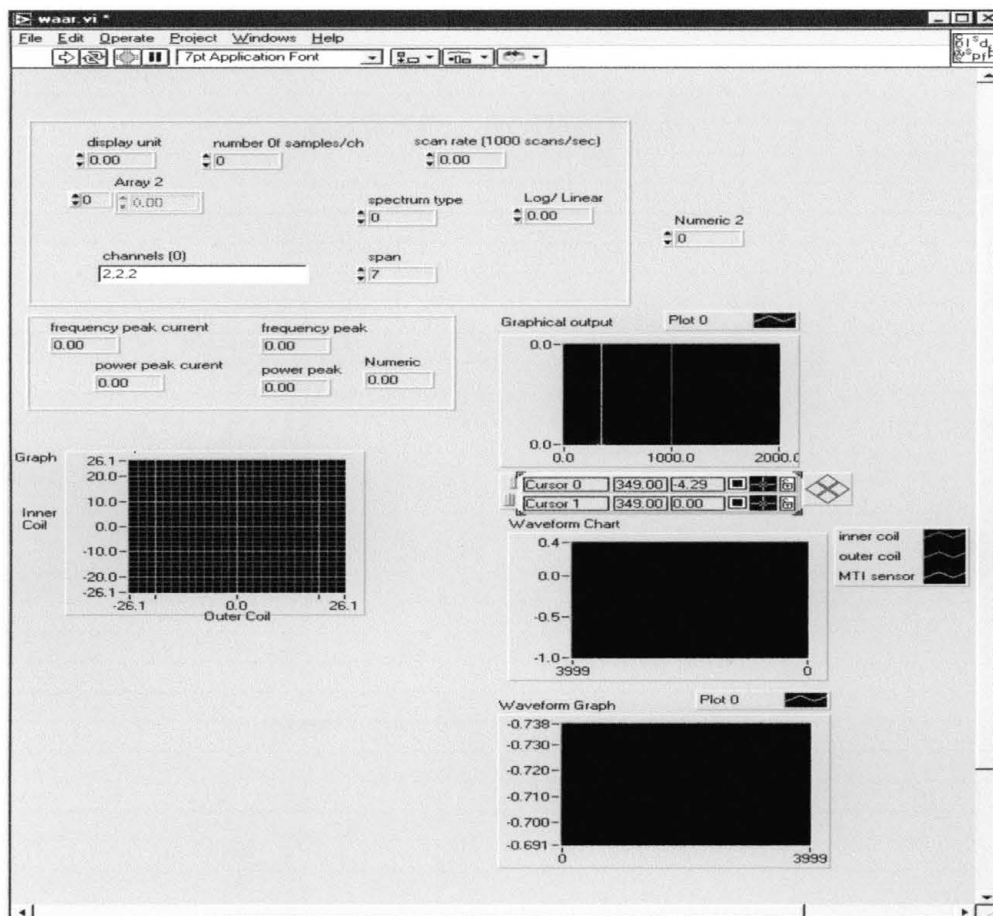


Figure 25: The Front panel of the Lab-View Program “WAAR.”

The remaining portion of the “WAAR” program uses various VI’s to compute the peak frequency and power from the column of data of the deflection signal from the *MTI Sensor* and the maximum peak current in the *Inner and Outer Coils*.

The data from the “WAAR” program are the basis for computing the experimental coefficients in the “Direct Magnetostriction” program. The signal produced by the input channels 0 and 1 are analyzed by the object-oriented program, Figure 24, and the results are displayed on the front panel of Figure 25. The data from the *Inner and Outer Coils*, peak current

and peak power is used to compile the numerical data, which represent the magnetic field emanating from both the inner and outer Helmholtz Coils [8].

CHAPTER 6

MEASURED RESULTS

6.1 MAGNETO-ELASTIC EFFECTS: GROUND WORK FOR MAGNETOSTRICTION MEASUREMENT

The preliminary results of the magnetostriction measurement technique for various film thickness was to determine not only to see if the technique was applicable for measuring thin and ultra thin ferromagnetic film, but also to substantiate the fact that material with high magneto-elastic effects have high magnetostriction.

The experiment conducted by a colleague Patrick Holland, measured how the magnetic hysteresis of the film NiFe on a glass/Ti substrate was found to undergo changes to its magnetic properties as a function of an externally applied stress.

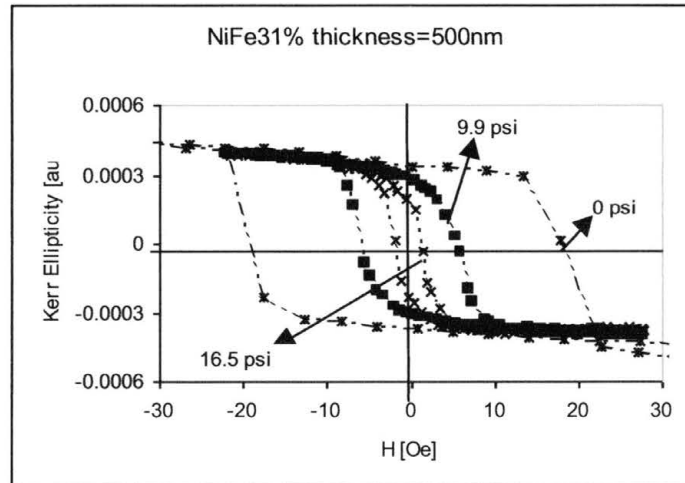


Figure 26: The Magneto-elastic Effect of a 500nm thick 31% NiFe sample.

The hysteresis curve of a 500 nm thick 31% NiFe sample for different values of an applied tensile stress is shown in Figure 26. The dashed curve represents the hysteresis curve when no stress is applied to the sample. The measured results indicate that the coercivity and hysteresis is largest when no stress is applied to the film. Tensile stress is applied to the sample and the coercivity or intensity of the applied field required to reduce the magnetization of the sample to zero after the magnetization of the sample is driven to saturation decreases. The coercivity is a measure of the degree of magnetic hysteresis and therefore characterizes the loss of soft magnetic materials. The hysteresis loss, i.e. the enclosed area of the hysteresis curve, decreases clearly with increased tensile stress.

The conclusion based on the data of the hysteresis curve is that the magnetic properties of the sample depend largely on the applied stress, thus the material is highly magneto-elastic.

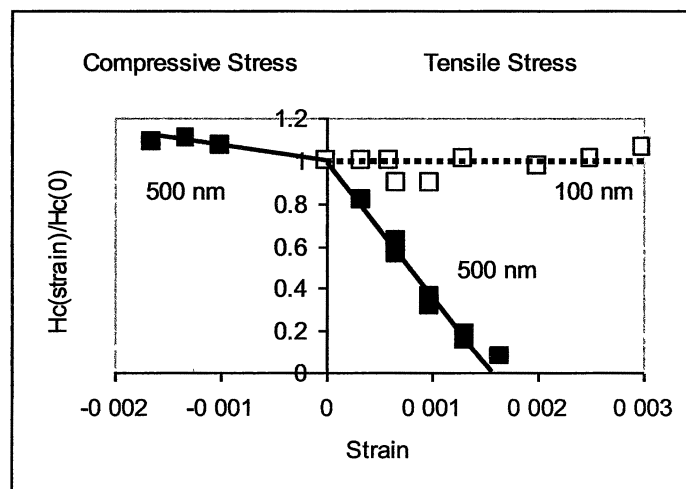


Figure 27: The Magneto-elastic Effect for Thin and Thick Ferromagnetic Film.

Figure 27 depicts the changes in the coercivity as a function of the applied stress for two ferromagnetic samples of different thickness. The black rectangular boxes represent the data

for the thick film while the white boxes represent the data from the thin film. Based on the data it was concluded that the thick film is very magneto-elastic. However, the hysteresis of the thin film appears to be independent of the applied stress.

Since the magneto-elastic properties of soft magnetic material largely depend on its magnetostriction, it was concluded that an experimental process needed to be erected that would measure the magnetostriction for a multitude of samples of varying thickness.

6.2 PRELIMINARY RESULTS OF MAGNETOSTRICTION FOR VARIOUS FILM THICKNESSES

I used the setup described in chapter 5 to measure the samples of colleague Patrick Holland. Fig. 29 shows a sequence of data of varying film thickness of 31% Ni-Fe on a Si/SiO₂ (2nm) substrate. The samples thickness ranges from 100 to 543 nm.

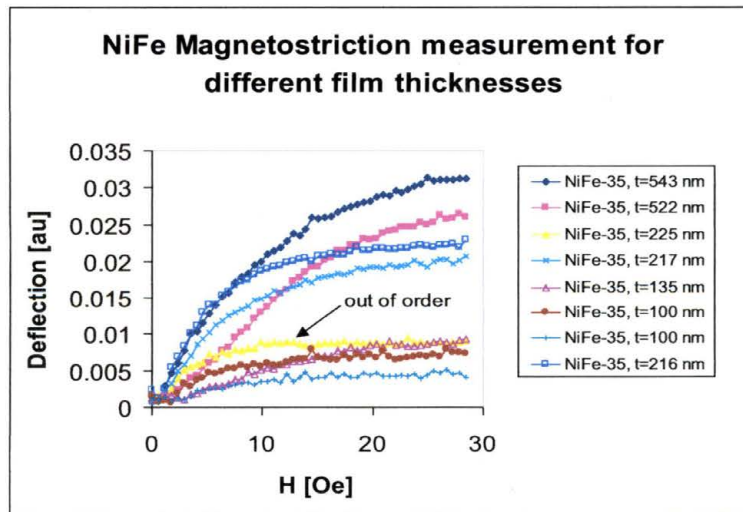


Figure 18: Hysteresis curve of the Deflection of various samples of 31% sample of NiFe.

The data in Figure 29 shows the thicker the film the larger the numerical deflection value. An exception is the data of the 225 nm film which is out of order⁴.

Notice that deflection of the thinnest film was less than 15 A. As the guaranteed resolution of the Fotonic sensor is only 2.5 A it is clear that the measured deflections contain random and systematic errors.

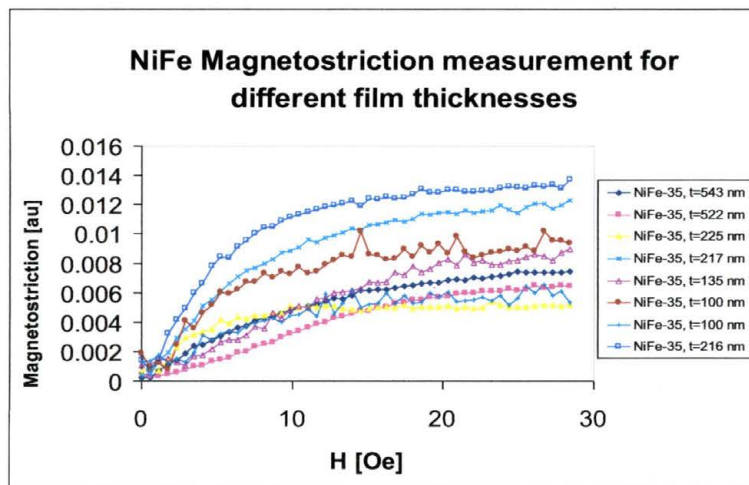


Figure 19: The Measured Deflection as a function of applied fields for various samples of 31-NiFe.

Figure 30 is the magnetostriction value determined from the measured deflection.

The bottom three curves are films whose thicknesses are 225 nm, 100 nm and 522 nm.

Experimentally the expected value of the order of magnetostrictive values should exhibit consistency through out the experimental process, yet based on Figure 30 this is not the case. Therefore there exist other reasons other than those mentioned earlier for the numerical errors associated with the experimental magnetostriction results. In addition to the reason mentioned above there are three other factors that cause errors in the calculated magnetostriction:

⁴ It shall be noted that the exception is the 225 nm thick film and as a result is out of order.

- a. The thickness of the substrate is not exactly known. Measurements of the thickness of different SiO_2 substrates with the CV technique by Dunn showed a variation of at least 5%.
- b. The film thickness is not conclusive. The samples were cut from large SiO_2 wafer segments greater 2 to 3 inch in diameter and therefore the deposition rate of the magnetron sputtering system used is not constant over such large area. The film thickness is estimation from the deposition time and rate and hasn't been verified. It is believed that variations in the film thickness from sample to sample may be as large as 30%.
- c. The thinner films have a larger coercivity and cannot be saturated by a magnetic field of 30 Oe. The data in Figure 30 also suggests that not all samples have the same coercivity or saturation field (anisotropy field). The coercivity as a function of the film thickness in comparisons to those of lower coercivity is shown in Figure 31.

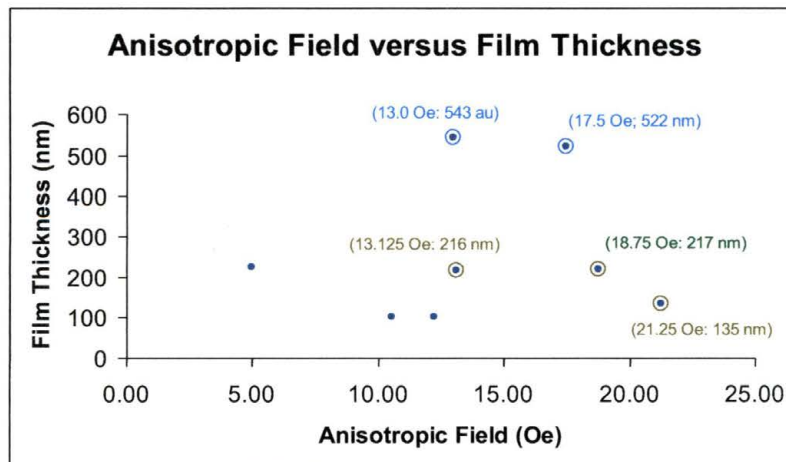


Figure 20: Anisotropic Field versus Film Thickness.

CHAPTER 7

CONCLUSION

A setup has been constructed that allows the determination of the magnetostriction from thin ferromagnetic films. The setup applies a rotating in-plane magnetic field to the sample, which causes the sample to vibrate with a frequency of twice the angular frequency of the magnetic field. The setup measures the amplitude of the vibration with a resolution down to 2.5 Angstrom.

The setup automatically calculates the magnetostriction coefficient from the elastic properties and thickness of both the film and substrate. The accuracy in the magnetostriction coefficient depends on the thickness of the substrate and the thickness of the film.

A 2nd hand stereo audio amplifier of \$200 was sufficient enough to supply power to Helmholtz coils compared to a \$7000 bipolar power supply.

The setup has demonstrated the ability to experimentally determine the variation of the magnetostriction with the film thickness in the event variation is smaller than measurement error. It should be noted though that the measurement error associated with the experiment values is based on the following: (a) the thickness of the substrates and films are not conclusive; (b) the Si substrate is relatively thick resulting in very small deflections; (c) the maximum applied magnetic field is not large enough to saturate the thinnest films.

In order to conclude whether or not the thickness dependence of the magneto-elastic properties depends on the thickness dependence of the magnetostriction additional experiments should be carried out. A new series of films needs to be deposited on thinner or

more flexible substrates and hence a larger deterministic value for the deflection. Thinner Si substrates are commercially available, however it might be viable to use thin microscope slides as substrates since they are more flexible than Si.

The maximum field that can be applied with the setup needs to be increased. This is possible if a stronger power supply is available. Although the maximum DC field that the Helmholtz coils can provide is approximately 50 Oe, it is possible to use a pulsating current and use the heat capacity of the Helmholtz coil to avoid the coils from being damaged. Since this particular experiment was completed other students have successfully applied this technique to do measurements in fields as high as 175 Oe, which for the record is much larger than the field available in commercial setups.

APPENDIX 1

OTHER PROPERTIES OF THE NICKEL IRON SYSTEM

The figures below show how the resistance, the magneto-resistance, and the initial permeability change as a function of the nickel concentration for the NiFe system

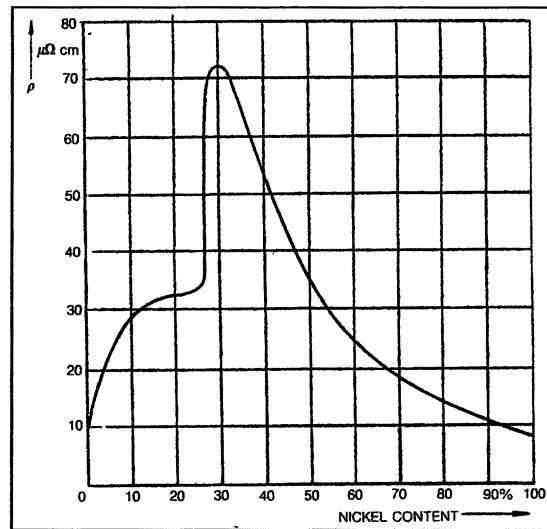


Figure 21: The change of resistivity as a function of nickel concentration for NiFe [16]

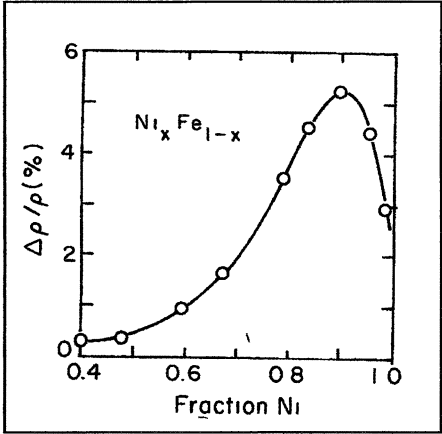


Figure 22: The change of magnetoresistance as a function of the nickel concentration for NiFe [18].

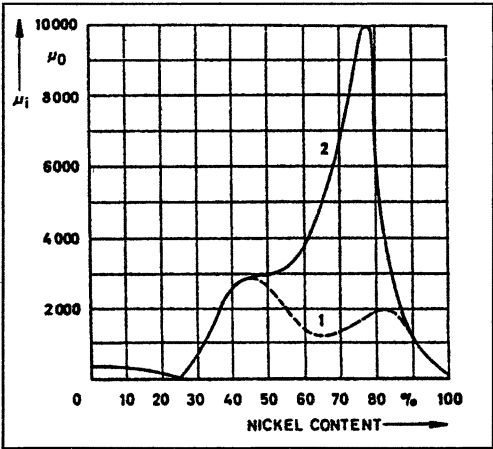


Figure 23: Change of the initial permeability as a function of the nickel concentration for NiFe [16]

APPENDIX 2

SELF-RESONANCE COIL: HIGH FREQUENCY LIMITATIONS OF HELMHOLTZ COIL

All electrical circuits have a limitation as to the range of frequencies it can endure. Essentially from an electrical circuit viewpoint a spool of magnetic wire will exhibit the same characteristics of an inductor and for this reason contain a small amount of parasitic capacitance. Therefore the electrical characteristics of the coils change as the external frequency of operation is increased.

The parasitic capacitance of the coils at high frequencies reduces the measure of frequency range or bandwidth of the circuit and increases the susceptibility to interference. For the measured magnetostriction of each set of sample data, it is essential that the bandwidth be as broad as experimentally possible to achieve a measure of saturation for the various samples. And because the inductive properties of the coil will increase as the frequency is raised, the impedance will grow larger numerically and the inductor will eventually self-resonate.

In addition too the model self-resonating due to changes in the impedance of the inductance of the circuit will also self-resonate due too propagation effects.

The propagation effects are the result of finite velocity of the electron propagating thru the copper winding.

For a single bundle of magnetic copper windings operating at a frequency that is a significant fraction of the wavelength in circumference will cause the reactive circuit model to resonate at increased frequencies.

The result of skin depth, resistance and inductance must be taken into account during the experimental measurement process. It is these electrical characteristics that will result in parasitic behavior of the coils as the frequency of the incoming propagating signal is increased [11].

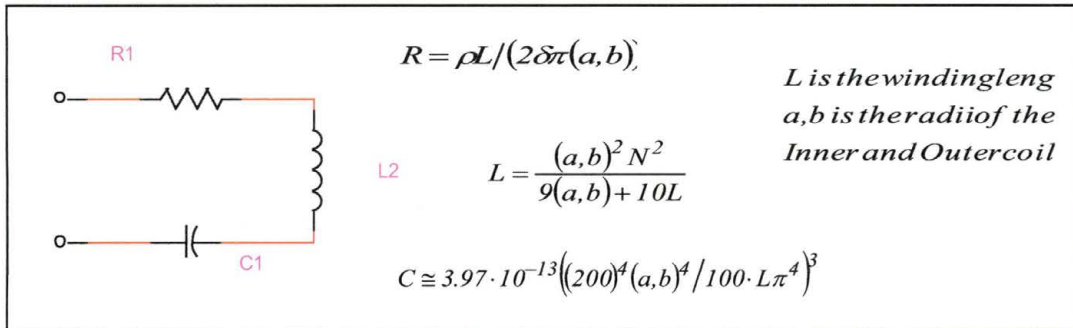


Figure 24: Self Resonance Circuit to emulate behavior of Helmholtz coil at high frequency.

BIBLIOGRAPHY

1. Victor H. Guerrero and Robert C. Wetherford. "Magnetostriction bending of cantilever beams and plates." Journal of Applied Physics 94:10 (2003): 6659-6663.
2. Ivan Cimrak. "On the Landau-Lifshitz Equation of Ferromagnetism." Department of Mathematics, Ghent University, 2005.
3. Xiaobo Tan, John S. Baras, P. S. Krishnaprasad. "Computational micromagnetics for Magnetostriction actuators." Institute for Systems Research, University of Maryland, College Park, MD, 2000.
4. David J. Griffith "Introduction to Electrodynamics 2nd Edition." Upper Saddle River, New Jersey. Prentice-Hall, 1989.
5. John David Jackson. "Classical Electrodynamics 3rd Edition." University of California, Berkeley. John Wiley and Sons, 1998.
6. Meilikhov. "Magnetic Ordering in a Random System of Point Ising Dipoles." Journal of Experimental and Theoretical Physics 97:3 (2003): 587-592.
7. Static: Strain Types: "A Scalable Tight-Binding Total Energy Evaluation Code," Center for Computational Materials. Naval Research Laboratory. Washington, DC.
8. E. W. Bogart, Mei. "Magnetostriction in thin Ferromagnetic layers for Applications in Data-Heads." Technische Universiteit, Eindhoven, Netherlands, 2000.
9. Satish S. Udpa, Patrick O. Moore. "Electromagnetic Testing." American Society for Non-Destructive Testing, 2004.
10. Sergey Loyka. "Information Theory and Electromagnetism: Simple Transmission Line Representation of Tesla Coil and Tesla's Wave Guides." Microwave Review 11:2 (2005).
11. Todd P. Meyrath. Center for Nonlinear Dynamics, (2001-2004).
12. D. Sander. "The Correlation between mechanical stress and magnetic anisotropy in ultrathin films." Reports on Progress in Physics 62 (1999): 809-858.
13. Patrick Holland. "Magnetic hysteresis curves of thin films under isotropic stress." 2001.

14. Claude Garrett, Patrick Holland, Wilhelmus J. Geerts, Dustin Ragan, Archana Dubey, Steve Rios, Anup K. Bandyopadhyay. "Thickness Dependence of the Magnetic Hysteresis of NiFe-31% Films as a Function of an Applied Isotropic In-plane Stress." Journal of Applied Physics 93 (May 2003): 8624.
15. Patrick Holland, Mary Kempton, Dustin Ragan, Steve Rios, Anup K. Bandyopadhyay, Archana Dubey, Wilhelmus J. Geerts, "Magnetic Hysteresis Measurements of Thin Films of NiFe-31% under Isotropic Stress." Journal of Magnetic Material 250 (2002): L1-L5.
16. David Jiles. "Introduction of Magnetism and Magnetic Materials." London: Chapman and Hall, 1991.
17. Gerald F. Dionne. "Conditions for stress-induced uniaxial anisotropy in magnetic materials of cubic symmetry." Materials Research Bulletin 6 (1971): 805-816.
18. Christoph Pohl. "Topics in Magnetism III. Hysteresis and Domains." Department of Physics College of William and Mary. Williamsburg, Virginia, 1982.
19. Ten, Brinke and Sombroek. A Scanning Kerr Microscope for Quantitative Domain Studies on Magnetic Thin Films. Texas State University. San Marcos, Texas.